

# Digital Twin-Empowered Deep Reinforcement Learning for Intelligent VNF Migration in Edge-Core Networks

Faisal Ahmed\*, Suresh Subramaniam<sup>‡</sup>, Motoharu Matsuura\*\*, Hiroshi Hasegawa<sup>††</sup>,  
and Shih-Chun Lin\*

\*North Carolina State University, Raleigh, NC, USA, {fahmed5, slin23}@ncsu.edu

<sup>‡</sup>The George Washington University, Washington, USA, suresh@gwu.edu

\*\*University of Electro-Communications, Chofu, Japan, m.matsuura@uec.ac.jp

<sup>††</sup>Nagoya University, Nagoya, Japan, hasegawa@nuee.nagoya-u.ac.jp

**Abstract**—The growing demand for services and the rapid deployment of virtualized network functions (VNFs) pose significant challenges for achieving low-latency and energy-efficient orchestration in modern edge-core network infrastructures. To address these challenges, this study proposes a Digital Twin (DT)-empowered Deep Reinforcement Learning framework for intelligent VNF migration that jointly minimizes average end-to-end (E2E) delay and energy consumption. By formulating the VNF migration problem as a Markov Decision Process and utilizing the Advantage Actor-Critic model, the proposed framework enables adaptive and real-time migration decisions. A key innovation of the proposed framework is the integration of a DT module composed of a multi-task Variational Autoencoder and a multi-task Long Short-Term Memory network. This combination collectively simulates environment dynamics and generates high-quality synthetic experiences, significantly enhancing training efficiency and accelerating policy convergence. Simulation results demonstrate substantial performance gains, such as significant reductions in both average E2E delay and energy consumption, thereby establishing new benchmarks for intelligent VNF migration in edge-core networks.

**Index Terms**—Digital Twin, Advantage Actor-Critic, VNF Migration, Edge-Core Network, VNF-FG

## I. INTRODUCTION

Network Function Virtualization (NFV) [1] marks a paradigm shift in network architecture, designed to lower operational costs by decoupling network functions (NFs) from specialized hardware appliances, such as conventional middle-boxes. By abstracting these NFs into software-based entities, namely, Virtualized Network Functions (VNFs) [2], NFV enables their deployment on general-purpose commodity servers. These deployments typically consist of ordered chains of VNFs including elements such as load balancers and firewalls. This architectural flexibility facilitates faster service provisioning, enhances scalability, optimizes resource utilization, and reduces operational expenditures for service providers [3].

However, as the adoption of NFV expands and the number of VNFs increases, scaling the VNF forwarding graph (VNF-FG) within edge networks becomes increasingly challenging

due to their limited computational resources. In contrast, core networks typically possess abundant computing capacity [4], making them well-suited for offloading VNFs from the edge. Integrating edge and core infrastructures into a unified edge-core network architecture thus offers enhanced flexibility for optimizing end-to-end delay (E2E) and improving overall service performance [4]. Nevertheless, this shift toward large-scale, distributed architectures brings forth additional challenges, most notably, the need to ensure a stable and reliable power supply. Given that energy consumption accounts for a significant share of operational expenditure, its intelligent and adaptive management is essential for achieving sustainable network growth [5]. In response, Network Service Providers are actively pursuing strategies to reduce the energy consumption of these infrastructures, with the overarching goal of enhancing operational efficiency [6].

Recently, significant research efforts have focused on optimizing the scheduling of VNFs, particularly deployment and migration strategies [3], [4], [7] to minimize E2E delay [3] and reduce energy consumption [5], [8]. Various studies have proposed deployment strategies aimed at optimizing delay and energy consumption [3], [6]; however, these often rely on static VNF placement, assuming fixed network demands and unconstrained resource availability. Such assumptions undermine their applicability in real-world scenarios, where demand is dynamic and resource contention is common. To overcome these limitations, VNF migration [3], [9] has emerged as a more adaptive and robust solution. By enabling the flexible relocation of VNFs to more optimal servers while preserving application states, VNF migration allows network infrastructures to respond dynamically to changing workloads and resource conditions, ensuring service continuity and efficient resource utilization in heterogeneous environments [3].

In parallel, the increasing complexity and dynamism of modern networks have fueled interest in Machine Learning (ML) for intelligent network management [10]. Although widely used, supervised ML often requires labeled data and struggles with uncertainty. In contrast, many networking tasks involve sequential decision-making under uncertainty, making Reinforcement Learning (RL) a more suitable paradigm [7]. Specifically, RL has proven effective in optimizing the orchestration of VNF-FGs across heterogeneous infrastructures, particularly in response to fluctuating service demands. Building upon this foundation, Deep Reinforcement Learning (DRL)

This work was supported in part by the National Science Foundation (NSF) under Grant CNS-221034, Meta 2022 AI4AI Research, and the NC Space Grant.

[7] combines RL with deep neural networks (DNNs) to tackle complex problems in high-dimensional spaces. DRL has shown great potential in tasks such as VNF migration in edge and core networks, where real-time decisions and efficient use of resources are crucial.

Although DRL has demonstrated notable performance improvements, it is typically implemented to solve large action spaces in tasks such as VNF migration and requires a substantial amount of training data. This, in turn, necessitates frequent interactions with the physical environment to collect sufficient data, imposing considerable overhead on real-world systems. To mitigate the burden a Digital Twin (DT) can be implemented to simulate environment dynamics and generate additional training data [11]. By serving as a virtual replica of the physical system, the DT enables the creation of a virtual experience buffer that, when combined with the physical experience buffer enriches the training dataset and accelerates policy convergence while reducing real-world exploration costs.

Building on the aforementioned insights, this study proposes a novel DT-empowered DRL framework for VNF migration in edge-core networks. The key contributions of this work are summarized as follows:

- To enhance the performance of the DRL model, specifically the Advantage Actor-Critic (A2C) for intelligent VNF migration within edge-core networks, a novel integration with a DT is proposed. This integration significantly reduces the reliance on physical environment interactions, thereby lowering system overhead.
- The DT module is composed of a multi-task Long Short-Term Memory (LSTM) network and a multi-task Variational Autoencoder (VAE). The multi-task LSTM continuously adapts to the environment by predicting state transition dynamics and reward feedback, while the multi-task VAE generates simulated state-action pairs. Together, the multi-task LSTM and VAE augment the training dataset by storing synthetic experiences in the DT experience buffer, thereby enhancing the training efficiency of the A2C model.
- The proposed framework is applied to solve the joint optimization problem of minimizing both the E2E delay of VNF-FGs and the energy consumption in edge-core networks.
- Extensive simulations demonstrate that the proposed framework significantly outperforms baseline methods. For example, in terms of average E2E delay and average energy consumption, the proposed framework achieves reductions of 7% and 15%, respectively, compared to baselines such as threshold-based VNF migration.

## II. SYSTEM MODEL AND PROBLEM FORMULATION

The considered edge-core network is modeled as a weighted undirected graph  $\Omega = (\mu, \nu)$ , where  $\mu$  denotes the set of servers and  $\nu$  represents the set of connectivity links between them. The server set is partitioned as  $\mu = \mu_e \cup \mu_c$ , where  $\mu_e = \{s_1, s_2, \dots, s_e\}$  represents the subset of edge cloud servers, and  $\mu_c = \{s_{e+1}, \dots, s_c\}$  corresponds to the subset of core cloud servers. Here,  $s_1 \leq s \leq s_e$  indexes the edge cloud servers, and  $s_{e+1} \leq s \leq s_c$  indexes the core cloud servers. The network architecture is assumed to include multiple levels of switching infrastructure to facilitate inter-server connectivity. Each link  $l \in \nu$  connects a pair of distinct servers, such as  $s_{e+1}$  and  $s_c$ , where  $s_{e+1}, s_c \in \mu_c$  and  $s_{e+1} \neq s_c$ . Each server  $s \in \mu$  is characterized by its available computational resources, namely memory and CPU. Let  $\zeta_s^{MEM}$  and  $\zeta_s^{CPU}$  denote the memory and CPU capacities

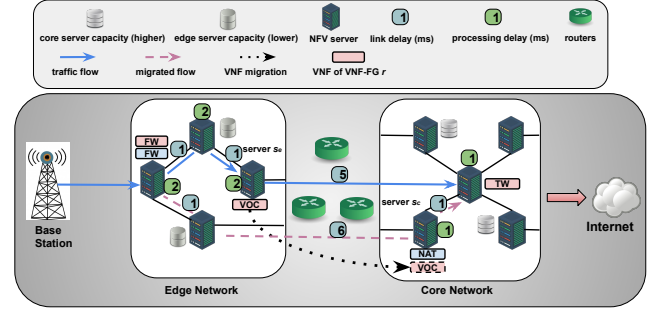


Figure 1. A representative example of an 8K video streaming service served by a VNF-FG demonstrates that the E2E delay is reduced from 14 ms to 12 ms, and the edge server  $s_e$  is powered off following VNF migration, thereby reducing overall energy consumption.

of server  $s$ , respectively. It is assumed that core cloud servers offer greater computational resources, whereas edge servers operate with comparatively limited capacity. Additionally, each connectivity link  $l = (s_{e+1}, s_c) \in \nu$  has an associated available bandwidth denoted by  $\zeta_l^{BW}$ .

To accommodate dynamic network conditions, the NFW system is assumed to operate in a time-slotted manner. Each service request, represented as a VNF-FG  $r \in R$ , comprises a set of VNFs, denoted by  $V_r = \{v_1, v_2, \dots, v_p\}$ , with each VNF deployed on each  $s \in \mu$  according to the strategy defined in [9]. At each time step  $t$ , each VNF  $v$  has an associated resource demand characterized by memory, CPU, and bandwidth requirements. The memory and CPU demands of VNF  $v$  in request  $r$  are denoted by  $\chi_{r,v}^{MEM}(t)$  and  $\chi_{r,v}^{CPU}(t)$ , respectively. In addition, the bandwidth requirement between any pair of connected VNFs, such as  $v_1$  and  $v_2$ , is represented by  $\chi_{r,\bar{l}}^{BW}(t)$ , where  $\bar{l}$  denote a logical link between the two VNFs and  $\bar{l} \in \bar{L}_r$ .

### A. VNF and Logical Link Mapping in VNF-FG, Associated Constraints, and Service Status

To begin with, two binary variables are introduced to represent the mapping status of VNFs and logical links within a VNF-FG  $r$  at time step  $t$ .

$$y_{r,v}^s(t) = \begin{cases} 1, & \text{server } s \text{ serves VNF } v \text{ at } t \\ 0, & \text{otherwise.} \end{cases} \quad (1)$$

$$z_{r,\bar{l}}^l(t) = \begin{cases} 1, & \text{link } l \text{ serves logical link } \bar{l} \text{ at } t \\ 0, & \text{otherwise.} \end{cases} \quad (2)$$

Even if a server  $s$  hosts at least one VNF, it must be activated to perform its functions; the same applies to a link  $l$ . Therefore, binary variables are introduced to indicate whether a server  $s$  and a link  $l$  are active at time step  $t$ .

$$x^s(t) = \begin{cases} 1, & \sum_{r \in R} \sum_{v \in V_r} y_{r,v}^s(t) \geq 1, s \in \mu \\ 0, & \text{otherwise.} \end{cases} \quad (3)$$

$$x^l(t) = \begin{cases} 1, & \sum_{r \in R} \sum_{\bar{l} \in \bar{L}_r} z_{r,\bar{l}}^l(t) \geq 1, l \in \nu \\ 0, & \text{otherwise.} \end{cases} \quad (4)$$

To ensure that sufficient resources are available on both servers and links when servicing VNF-FGs, the following

constraints are defined:

$$\sum_{r \in R} \sum_{v \in V_r} y_{r,v}^s(t) \cdot \chi_{r,v}^{CPU}(t) \leq \zeta_s^{CPU}, \quad s \in \mu \quad (5)$$

$$\sum_{r \in R} \sum_{v \in V_r} y_{r,v}^s(t) \cdot \chi_{r,v}^{MEM}(t) \leq \zeta_s^{MEM}, \quad s \in \mu \quad (6)$$

$$\sum_{r \in R} \sum_{l \in L_r} z_{r,l}^l(t) \cdot \chi_{r,l}^{BW}(t) \leq \zeta_l^{BW}, \quad l \in \nu \quad (7)$$

Each VNF-FG  $r \in R$  is associated with a service time  $\sigma_r^{serv}$ , representing the duration for which  $r$  is expected to remain active, provided that all its constituent VNFs are successfully placed while satisfying all system constraints, otherwise,  $\sigma_r^{serv}$  is set to zero. Accordingly, the service status of VNF-FG  $r$  at time step  $t$  is defined as:

$$\Phi_r(t) = \begin{cases} 1, & \sigma_r^{ariv} \leq t < (\sigma_r^{ariv} + \sigma_r^{serv}), \forall t \in T, r \in R \\ 0, & \text{otherwise,} \end{cases} \quad (8)$$

where,  $\sigma_r^{ariv}$  denotes the arrival time of the VNF-FG  $r$ .

### B. E2E Delay Model

The E2E delay experienced by a VNF-FG consists of three main components: propagation delay, transmission delay, and processing delay. Drawing on the studies in [12] and [13] the delay incurred on a physical link  $l$  for a VNF-FG  $r$  at time step  $t$  can be expressed as:

$$D_{link}^l(t) = D_{trans}^l(t) + D_{prop}^l(t), \quad l \in \nu, r \in R \quad (9)$$

here,  $D_{trans}^l(t)$  and  $D_{prop}^l(t)$  represent the transmission delay and propagation delay, respectively, at time step  $t$ .

Moreover, the processing delay at server  $s$  at time step  $t$  can be denoted as:

$$D_{proc}^s(t) = \frac{\Gamma_{CPU}^s(t) \cdot \tau}{1 - \Gamma_{CPU}^s(t)}, \quad s \in \mu, r \in R \quad (10)$$

where,  $\tau$  denotes the baseline processing delay per data packet, and  $\Gamma_{CPU}^s(t)$  is the CPU utilization of server  $s$  at time step  $t$ , defined as:

$$\Gamma_{CPU}^s(t) = \frac{\sum_{r \in R} \sum_{v \in V_r} y_{r,v}^s(t) \cdot \chi_{r,v}^{CPU}(t)}{\zeta_s^{CPU}}, \quad s \in \mu \quad (11)$$

Consequently, the total E2E delay for VNF-FG  $r$  at time  $t$  can be calculated as:

$$D_{E2E}^r(t) = \sum_{l \in L_r, l \in L_r} z_{r,l}^l(t) \cdot D_{link}^l(t) + \sum_{v \in V_r, s \in \mu} y_{r,v}^s(t) \cdot D_{proc}^s(t) \quad (12)$$

### C. Energy Consumption Model

The CPU is the primary source of server energy consumption, with its power usage assumed to scale linearly with utilization. Inspired by the energy consumption models presented in [14] and [8], the total energy consumption of server  $s \in \mu$  that hosts VNF  $v \in V_r$  from VNF-FG  $r \in R$  at time step  $t$  is given by:

$$E_s(t) = y_{r,v}^s(t) \cdot (\varepsilon_{base}^s(t) + \varepsilon_{cons}^s(t) \cdot \Gamma_{CPU}^s(t)) + \varepsilon_{trans}^s(t), \quad (13)$$

here,  $\varepsilon_{base}^s(t)$  denotes the baseline energy consumption of server  $s$ , while  $\varepsilon_{cons}^s(t)$  represents the incremental energy consumption per unit of CPU utilization, defined as,  $\varepsilon_{cons}^s(t) = \varepsilon_{max}^s(t) - \varepsilon_{base}^s(t)$ , where,  $\varepsilon_{max}^s(t)$  denotes the maximum energy consumption when server  $s$  operates at full CPU capacity. In addition,  $\varepsilon_{trans}^s(t)$  represents the transition energy consumption of server  $s$  at time step  $t$ . This transition energy consumption accounts for the power overhead associated with changes in the server's operational mode, such as transitioning from a sleep mode to an active mode due to VNF migration. If the operational mode of server  $s$  remains unchanged between time steps  $t-1$  and  $t$ , the transition energy consumption is assumed to be zero, that is,  $\varepsilon_{trans}^s(t) = 0$ .

### D. Problem Formulation

The primary objective of this study is to maximize the reduction of both the E2E delay of VNF-FGs and the energy consumption in edge-core network through VNF migration. Consider, for example, a service request for 8K video streaming that is processed by a sequence of VNFs in a VNF-FG  $r \in R$ , such as a firewall (FW), traffic monitor (TM), and video optimization controller (VOC) at time step  $t$ . As illustrated in Figure 1, the E2E delay is reduced from 14 ms to 12 ms when the VOC is migrated from an edge cloud server  $s_e$  to a core cloud server  $s_c$ . Furthermore, since edge cloud server  $s_e$  no longer hosts any VNFs, it can be powered off, thereby contributing to a reduction in the overall energy consumption of the network.

The reduction in E2E delay resulting from VNF migration is denoted as:

$$\delta(t) = \Upsilon - \Upsilon' \quad (14)$$

where,  $\Upsilon$  refers to the E2E delay before VNF migration, and  $\Upsilon'$  denotes the E2E delay after migration.

Similarly, the reduction in energy consumption due to VNF migration is given by:

$$\eta(t) = \Lambda - \Lambda' \quad (15)$$

where,  $\Lambda$  represents the total energy consumption of the network before migration, and  $\Lambda'$  denotes the energy consumption after migration.

Since the objective is to jointly maximize the reduction in both E2E delay and energy consumption, a unified variable is defined by combining the two metrics with corresponding weighting coefficients. This composite variable, derived from Eq. (14) and (15), is expressed as:

$$\lambda = (\tau_1 \cdot \delta(t) + \tau_2 \cdot \eta(t)), \quad (16)$$

where,  $\tau_1$  and  $\tau_2$  are weighting coefficients in the range  $[0, 1]$ . **Optimization 1.** For a set of  $R$  VNF-FGs over time steps  $t = 1$  to  $T$ , the VNF migration problem in the edge-core network is formulated as the maximization of the total average reduction in E2E delay and energy consumption:

$$\max \frac{1}{T} \sum_{t=1}^T \sum_{r \in R} \lambda, \quad \forall v \in V_r \quad (17)$$

subject to:

$$\mathbf{C1} : \text{Eq.(5) - Eq.(7),} \quad (18)$$

$$\mathbf{C2} : D_{E2E}^r(t) \leq D_{max}^r, \quad (19)$$

here,  $D_{max}^r$  denotes the maximum tolerable E2E delay for VNF-FG  $r$ .

### III. DT-EMPOWERED DRL FOR VNF MIGRATION

#### A. Key Procedures of the Proposed VNF Migration Scheme

The proposed VNF migration scheme operates as follows, with detailed descriptions of the DRL module and the DT module presented in the following subsections.

At the beginning of each time step  $t$ , the system scans all servers and links to remove timed-out VNF-FGs, i.e., those for which  $\Phi_r(t) = 0, \forall r \in R$ . Subsequently, if there are incoming VNF-FG requests at time step  $t$ , the system accepts all of them and performs VNF deployment according to [9]. Following this, the system employs the DT-empowered DRL framework to make decisions regarding VNF migration when necessary. Finally, the network configuration and the set of accepted requests are updated, marking the active VNF-FGs with  $\Phi_r(t) = 1$ .

#### B. Description of the DRL Module

Since **Optimization 1** constitutes a joint optimization problem that aims to maximize the reduction of both E2E delay and average energy consumption, it poses significant challenges for conventional optimization techniques due to its complexity and inherent non-convexity. To address this, we reformulate **Optimization 1** as a Markov Decision Process (MDP) and adopt the A2C algorithm to solve it effectively. The formulated MDP can be represented as  $\mathcal{M} = \{\mathcal{S}, \mathcal{A}, \mathcal{R}, \mathcal{P}\}$ , which includes the state space  $\mathcal{S}$ , the action space  $\mathcal{A}$ , the reward function  $\mathcal{R}$ , and the state transition probability  $\mathcal{P}$ . In practice, state transition probabilities are typically unknown, and A2C addresses this by learning through direct interaction with the environment.

In A2C, two separate deep neural networks, that is, actor and critic are implemented. The actor network outputs a stochastic policy  $\pi(\mathcal{A}|\mathcal{S}; \theta^\pi)$ , while the critic estimates the state value function  $V(\mathcal{S}; \theta^V)$ . The training leverages the advantage function defined as,  $A(\mathcal{S}, \mathcal{A}) = \mathcal{R} + \gamma V(\mathcal{S}'; \theta^V) - V(\mathcal{S}; \theta^V)$ , which captures how much better an action  $\mathcal{A}$  is compared to the expected value of the current state. This advantage term is used to guide policy updates, thereby reducing the variance of gradient estimates and accelerating convergence.

The actor loss is defined as:

$$L_{actor}(\theta^\pi) = -\mathbb{E}_{\mathcal{S}, \mathcal{A}} [\log \pi(\mathcal{A}|\mathcal{S}; \theta^\pi) \cdot A(\mathcal{S}, \mathcal{A})] \quad (20)$$

that encourages the policy to increase the probability of advantageous actions. The critic loss is computed as the mean squared error between the predicted and target value:

$$L_{critic}(\theta^V) = \mathbb{E}_{\mathcal{S}, \mathcal{R}, \mathcal{S}'} \left[ (\mathcal{R} + \gamma V(\mathcal{S}'; \theta^V) - V(\mathcal{S}; \theta^V))^2 \right] \quad (21)$$

This dual-network structure, combined with advantage-based updates, ensures stable and sample-efficient learning, making A2C well-suited for complex and high-dimensional optimization problems such as the one tackled in this study. The components of MDP, that is, state, action, and reward function are describe as follows:

**State:** At time step  $t$ , the system state is represented by a vector  $\mathcal{S}(t)$ , consisting of eight key components:  $\{\xi(t), \psi(t), \rho(t), \iota(t), \varphi(t), \varrho(t), \varpi(t), \varsigma(t)\}$ . Specifically,  $\xi(t)$  indicates whether each server is in active or sleep mode, while  $\psi(t)$  indicates whether each server is hosting at least one VNF, where  $\psi(t) = y_{r,v}^s(t)$ . The components  $\rho(t)$ ,  $\iota(t)$ ,  $\varphi(t)$ , and  $\varrho(t)$  represent the sets of CPU utilizations, memory utilizations, energy consumptions, and processing delays, respectively, for all servers  $s \in \mu$  at time step  $t$ . Additionally,  $\varpi(t)$  captures

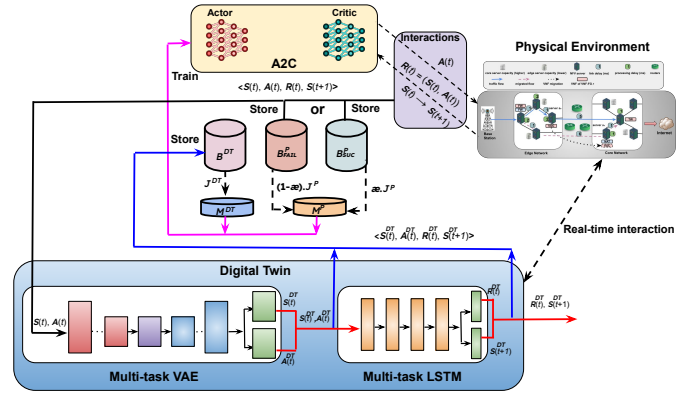


Figure 2. Operation of the DT-empowered DRL.

the server-level deployment mapping of VNFs for each VNF-FG  $r \in R$ , specifying which servers are hosting VNFs from  $r$  at time  $t$ . Finally,  $\varsigma(t)$  denotes the set of resource demands, specifically, the memory and CPU requirements associated with each VNF within its corresponding VNF-FG  $r$ .

**Action:** At time step  $t$ , the action taken by the system, denoted as  $\mathcal{A}(t)$ , represents the selection of servers from the set  $\mu$  for migrating VNFs associated with a VNF-FG  $r \in R$ , where,  $\mu = \mu_e \cup \mu_c$ , with  $\mu_e = \{s_1, s_2, \dots, s_e\}$  and  $\mu_c = \{s_{e+1}, \dots, s_c\}$ .

**Reward Function:** At time step  $t$ , the reward function for migrating VNFs associated with a VNF-FG  $r \in R$  is computed based on Eq. (16) as follows:

$$\mathcal{R}(\mathcal{S}(t), \mathcal{A}(t)) = \text{sigm}(\lambda), \quad (22)$$

here,  $\text{sigm}(\cdot)$  denotes the sigmoid function which is applied to normalize the reward within a bounded range.

#### C. Description of the DT Module

In this study, the training efficiency of the system is improved by establishing a DT of the physical environment. The digital twin focuses exclusively on modeling the environment's feedback to the system's actions, thereby simplifying its design and reducing the overhead typically associated with constructing a complete replica of the physical system. Within the DT framework, a multi-task VAE [15] is implemented to generate synthetic state-action pairs, while a multi-task LSTM [16] network is utilized to predict the corresponding next state and reward based on these outputs. This combination enables the DT to simulate realistic environment dynamics and augment the training process with high-quality synthetic data.

At time step  $t$ , the multi-task VAE model  $\mathcal{V}$  takes as input the physical environment's state  $\mathcal{S}(t)$  and action  $\mathcal{A}(t)$ , and generates the corresponding state and action in the DT, denoted as  $\mathcal{S}^{DT}(t)$  and  $\mathcal{A}^{DT}(t)$ . This process can be formally expressed as:

$$\mathcal{V}(\mathcal{S}(t), \mathcal{A}(t)) = \mathcal{S}^{DT}(t), \mathcal{A}^{DT}(t) \quad (23)$$

The loss function for the multi-task VAE is composed of a reconstruction term and a regularization term. It can be expressed as:

$$\mathcal{L}(\theta, \phi) = -\mathbb{E}_{z \sim q_\phi(z|x_{in})} \left[ \log p_\theta(\mathcal{S}^{DT}|z) + \log p_\theta(\mathcal{A}^{DT}|z) \right] + \text{KL}(q_\phi(z|x_{in}) \| p(z)), \quad (24)$$

where,  $x_{in} = (\mathcal{S}(t), \mathcal{A}(t))$  is the input to the encoder,  $q_\phi(z|x_{in})$  is the approximate posterior,  $p_\theta(\cdot|z)$  are the decoder likelihoods for state and action outputs, and  $p(z)$  is the prior distribution over latent variables. The Kullback–Leibler (KL) divergence term ensures that the learned latent distribution remains close to the prior.

Moreover, at time step  $t$ , the multi-task LSTM model  $\mathcal{T}$  utilizes the generated DT state  $\mathcal{S}^{DT}(t)$  and action  $\mathcal{A}^{DT}(t)$  as inputs to predict the next state  $\mathcal{S}^{DT}(t+1)$  and the corresponding reward  $\mathcal{R}^{DT}(t)$ , and can be expressed as:

$$\mathcal{T}(\mathcal{S}^{DT}(t), \mathcal{A}^{DT}(t)) = \mathcal{S}^{DT}(t+1), \mathcal{R}^{DT}(t) \quad (25)$$

The adopted loss function for the network is the mean squared error (MSE), can be formulated as:

$$\mathcal{L}_{MSE} = \kappa_1 \cdot \|\mathcal{S}^{DT}(t+1) - \mathcal{S}(t+1)\|^2 + \kappa_2 \cdot \|\mathcal{R}^{DT}(t) - \mathcal{R}(\mathcal{S}(t), \mathcal{A}(t))\|^2, \quad (26)$$

where,  $\kappa_1$  and  $\kappa_2$  are weighting coefficients, ranging from  $[0, 1]$ .

A DT experience buffer, denoted as  $\mathcal{B}^{DT}$  is established to store the generated data tuples, comprising  $\langle \mathcal{S}^{DT}(t), \mathcal{A}^{DT}(t), \mathcal{R}(\mathcal{S}^{DT}(t), \mathcal{A}^{DT}(t)), \mathcal{S}^{DT}(t+1) \rangle$ . This virtual experience buffer is utilized alongside the physical experience buffers to train the A2C model, thereby improving sample efficiency and accelerating policy convergence.

#### D. DT-Empowered DRL Framework Training

To train the A2C model, the DT experience buffer  $\mathcal{B}^{DT}$  and two physical experience buffers are utilized, namely, the successful physical experience buffer  $\mathcal{B}_{SUC}^P$  and the unsuccessful physical experience buffer  $\mathcal{B}_{FAIL}^P$ . Separating successful and unsuccessful experiences helps the system distinguish between constraint-satisfying and constraint-violating actions, enabling more informed policy updates than conventional random sampling. At each time step  $t$ , after executing an action, if the constraints **C1** and **C2** are not satisfied, the corresponding experience is stored in  $\mathcal{B}_{FAIL}^P$ ; otherwise, it is stored in  $\mathcal{B}_{SUC}^P$ . During each training iteration, the system randomly samples  $\kappa \cdot J^P$  experiences from  $\mathcal{B}_{SUC}^P$  and  $(1 - \kappa) \cdot J^P$  experiences from  $\mathcal{B}_{FAIL}^P$  to form the physical mini-batch  $M^P$ . The parameter  $\kappa \in [0, 1]$  controls the balance between successful and unsuccessful experiences and is critical for stable training. In the case of  $\mathcal{B}^{DT}$ , a DT mini-batch  $M^{DT}$  is formed by randomly sampling  $J^{DT}$  experiences from the  $\mathcal{B}^{DT}$ .

During the training iterations, the combined mini-batches  $M^P$  and  $M^{DT}$  are used to update the A2C model. It is important to note that the multi-task VAE and multi-task LSTM models within the DT are trained separately using experiences from  $\mathcal{B}_{FAIL}^P$  and  $\mathcal{B}_{SUC}^P$ . The overall training and interaction process is illustrated in Figure 2.

### IV. PERFORMANCE EVALUATION

#### A. Simulation Setup

A physical edge–core network is generated based on the Waxman topology model with parameters  $\alpha = 0.5$  and  $\beta = 0.2$ , following the configuration described in [17]. The network consists of 60 servers, with 20 designated as edge cloud servers and 40 as core cloud servers, as specified in [4]. The edge cloud servers are configured with 40 units of CPU resources and 16 units of memory resources, whereas the core cloud servers are configured with 200 units of CPU resources and 64 units of memory resources [4]. The CPU and memory utilization

thresholds are both set to 80%. Additionally, the available bandwidth for each link is set to 3.5 Gbps [12]. The CPU and memory resource demands for each VNF within the VNF-FGs are randomly assigned, ranging from 1 to 20 units for CPU and from 1 to 4 units for memory, consistent with [4]. Regarding server energy consumption, the baseline energy consumption is set to 10 units, the maximum energy consumption is set to 110 units, and the transition energy consumption is set to 2 units. Each VNF-FG is composed of four VNFs. In each episode, 300 VNF-FG requests arrive sequentially, following a Poisson process with an average arrival rate of 0.2 requests per time step. The packet rate within each VNF-FG is set to 100 packets per second.

In the A2C model, both the actor and critic networks are implemented as fully connected neural networks with three hidden layers comprising 256, 128, and 64 neurons, respectively, all using ReLU activation. The actor network outputs deterministic actions through a Tanh-activated layer with 64 neurons, while the critic network outputs a single Q-value via a linear neuron. In the DT module, the multi-task LSTM network comprises a single LSTM layer with 64 hidden units, followed by a fully connected layer with 64 ReLU-activated neurons. Its output is split into two task-specific heads: one predicts the next state, the other the immediate reward, both using linear activation. The multi-task VAE module includes an encoder with two ReLU-activated hidden layers of 64 and 32 neurons, followed by two output layers estimating the mean and log-variance of the latent distribution. The decoder consists of a shared hidden layer with 64 ReLU-activated neurons and two task-specific Sigmoid heads for reconstructing the digital twin state and action, respectively. Table I summarizes the simulation parameters used for the A2C model and associated neural networks.

Table I  
DRL AND DT PARAMETERS FOR SIMULATION

Parameters	Values
Successful experience buffer size ( $\mathcal{B}_{SUC}^P$ )	4000
Unsuccessful experience buffer size ( $\mathcal{B}_{FAIL}^P$ )	2000
Virtual experience buffer size ( $\mathcal{B}^{DT}$ )	6000
Balance parameter ( $\iota$ )	0.35
Learning rate of actor & critic	0.1
Discount factor ( $\gamma$ )	0.95
Physical mini-batch size ( $M^P$ )	32
DT mini-batch size ( $M^{DT}$ )	32
Optimizer	Adam

Furthermore, the Tensorflow-Keras platform is utilized to construct and train DNN models. Simulations are executed on a 2021 MacBook Pro, equipped with an Apple M1 Pro chip, featuring a 64-bit operating system, an 8-core CPU, a 14-core GPU, and 16GB of unified RAM.

For benchmarking performance comparisons, two VNF migration methods are examined, **(1) Threshold-based automatic VNF migration [9]**: The system monitors the CPU and memory utilization on servers and triggers VNF migration when either resource exceeds predefined thresholds, migrating VNFs from overutilized servers to underutilized servers criteria such as current running load. **(2) Random VNF migration**: The system randomly migrates VNFs within the edge–core network without considering any optimization criteria.

#### B. Numerical Results and Comparisons

Figure 3(a) illustrates that the proposed framework outperforms baseline approaches, such as the threshold-based



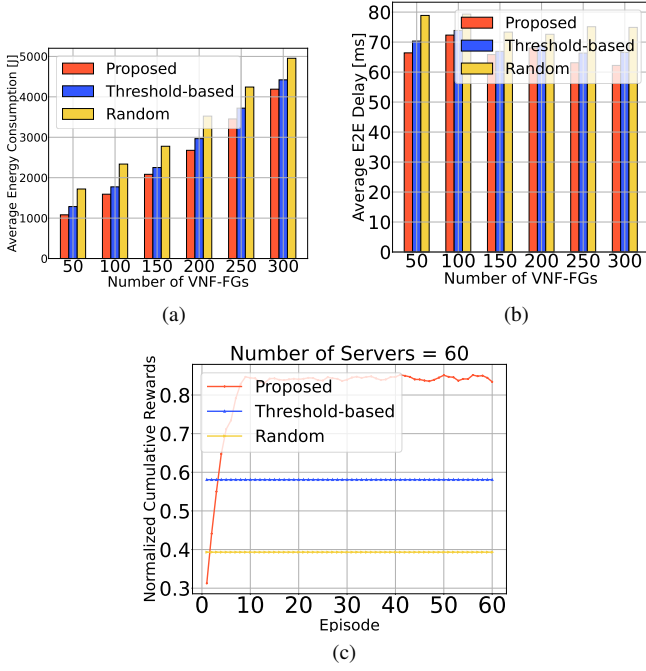


Figure 3. (a) Average energy consumption vs. number of VNF-FGs, (b) Average E2E delay vs. number of VNF-FGs, (c) Normalized cumulative rewards vs. episodes.

and random scheme, in terms of average energy consumption across varying numbers of VNF-FGs. Specifically, it achieves reductions of 15% and 29%, respectively. This improvement is attributed to the integration of A2C with a DT, which enables effective management of a high-dimensional state-action space and leads to higher cumulative rewards and lower energy use. In contrast, both baseline methods activate a larger number of servers during VNF migration, resulting in increased energy consumption.

Figure 3(b) presents the average E2E delay of the proposed framework compared to baseline approaches, such as the threshold-based and random scheme. The proposed method achieves the lowest average E2E delay, with reductions of 7% and 18%, respectively. This improvement stems from the reward function design in A2C, which jointly optimizes reductions in energy consumption and E2E delay before and after VNF migration.

Figure 3(c) shows that the normalized cumulative reward of the A2C model in the proposed framework achieves significantly faster convergence, stabilizing in as few as 12 episodes. In contrast, the baseline approaches, such as the threshold-based and random scheme exhibit no convergence behavior, as they are not learning-based methods.

## V. CONCLUSIONS

In this study, a novel Digital Twin (DT)-assisted Deep Reinforcement Learning (DRL) framework is proposed to enhance the efficiency and intelligence of VNF migration in edge-core networks. By integrating the Advantage Actor-Critic model with a DT that captures network dynamics through a multi-task Long Short-Term Memory network and a multi-task Variational Autoencoder, the proposed solution effectively achieves the objective of reducing both average end-to-end delay and energy

consumption. The incorporation of synthetic experience buffers alongside physical experience buffers further improves sample efficiency, enabling robust training even under highly dynamic workload conditions. Extensive evaluation demonstrates that the proposed framework consistently outperforms traditional threshold-based and random migration strategies across key performance metrics, such as average energy consumption, average E2E delay, and convergence speed. These findings validate the effectiveness of leveraging DT and DRL to enable scalable, adaptive, and sustainable orchestration of VNFs.

## REFERENCES

- [1] B. Yi, X. Wang, K. Li, S. K. Das, and M. Huang, "A comprehensive survey of network function virtualization," *Computer Networks*, vol. 133, pp. 212–262, 2018.
- [2] A. Laghrissi and T. Taleb, "A survey on the placement of virtual resources and virtual network functions," *IEEE Communications Surveys & Tutorials*, vol. 21, no. 2, pp. 1409–1434, 2019.
- [3] W. Liang, L. Cui, and F. P. Tso, "Low-latency service function chain migration in edge-core networks based on open jackson networks," *Journal of Systems Architecture*, vol. 124, p. 102405, 2022.
- [4] Q. Zhang, F. Liu, and C. Zeng, "Online adaptive interference-aware vnf deployment and migration for 5g network slice," *IEEE/ACM Transactions on Networking*, vol. 29, no. 5, pp. 2115–2128, 2021.
- [5] Y. Mu, L. Wang, and J. Zhao, "Energy-efficient and interference-aware vnf placement with deep reinforcement learning," in *2021 IFIP Networking Conference (IFIP Networking)*, 2021, pp. 1–9.
- [6] R. Sahraoui, O. Houidi, and F. Bannour, "Energy-aware vnf-fg placement with transformer-based deep reinforcement learning," in *NOMS 2024-IEEE Network Operations and Management Symposium*, 2024, pp. 1–9.
- [7] J. Pei, P. Hong, M. Pan, J. Liu, and J. Zhou, "Optimal vnf placement via deep reinforcement learning in sdn/nfv-enabled networks," *IEEE Journal on Selected Areas in Communications*, vol. 38, no. 2, pp. 263–278, 2020.
- [8] L. Tang, Z. Li, J. Li, D. Fang, L. Li, and Q. Chen, "Dt-assisted vnf migration in sdn/nfv-enabled iot networks via multiagent deep reinforcement learning," *IEEE Internet of Things Journal*, vol. 11, no. 14, pp. 25 294–25 315, 2024.
- [9] J. Fu and G. Li, "An efficient vnf deployment scheme for cloud networks," in *2019 IEEE 11th International Conference on Communication Software and Networks (ICCSN)*, 2019, pp. 497–502.
- [10] J. Xie, F. R. Yu, T. Huang, R. Xie, J. Liu, C. Wang, and Y. Liu, "A survey of machine learning techniques applied to software defined networking (sdn): Research issues and challenges," *IEEE Communications Surveys & Tutorials*, vol. 21, no. 1, pp. 393–430, 2018.
- [11] Z. Zhang, Y. Huang, C. Zhang, Q. Zheng, L. Yang, and X. You, "Digital twin-enhanced deep reinforcement learning for resource management in networks slicing," *IEEE Transactions on Communications*, vol. 72, no. 10, pp. 6209–6224, 2024.
- [12] Y. Yue, X. Tang, Y.-C. Liang, C. Cao, L. Xu, W. Yang, and Z. Zhang, "Deepselector: A deep learning-based virtual network function placement approach in sdn/nfv-enabled networks," *IEEE Transactions on Mobile Computing*, vol. 24, no. 3, pp. 1759–1773, 2025.
- [13] J. Pei, P. Hong, K. Xue, and D. Li, "Efficiently embedding service function chains with dynamic virtual network function placement in geo-distributed cloud system," *IEEE Transactions on Parallel and Distributed Systems*, vol. 30, no. 10, pp. 2179–2192, 2019.
- [14] F. Alharbi, Y.-C. Tian, M. Tang, W.-Z. Zhang, C. Peng, and M. Fei, "An ant colony system for energy-efficient dynamic virtual machine placement in data centers," *Expert Systems with Applications*, vol. 120, pp. 228–238, 2019.
- [15] G. Lu, X. Zhao, J. Yin, W. Yang, and B. Li, "Multi-task learning using variational auto-encoder for sentiment classification," *Pattern Recognition Letters*, vol. 132, pp. 115–122, 2020.
- [16] M. Karimzadeh, S. M. Schwegler, Z. Zhao, T. Braun, and S. Sargento, "Mtl-lstm: Multi-task learning-based lstm for urban traffic flow forecasting," in *2021 International Wireless Communications and Mobile Computing (IWCMC)*, 2021, pp. 564–569.
- [17] Z. Yan, J. Ge, Y. Wu, L. Li, and T. Li, "Automatic virtual network embedding: A deep reinforcement learning approach with graph convolutional networks," *IEEE Journal on Selected Areas in Communications*, vol. 38, no. 6, pp. 1040–1057, 2020.